Deorbitalized meta-GGA exchange-correlation functionals in solids

Daniel Mejia-Rodriguez and S. B. Trickey

Deorbitalized meta-GGA Exchange-Correlation Functionals in Solids

Daniel Mejia-Rodriguez[1, *] and S.B. Trickey[2, †]

[1] *Quantum Theory Project, Department of Physics, University of Florida, Gainesville, FL 32611*
[2] *Quantum Theory Project, Departments of Physics and of Chemistry, University of Florida, Gainesville, FL 32611*

(Dated: 20 July 2018; revised 29 Aug. 2018)

A procedure for removing explicit orbital dependence from meta-generalized-gradient approximation (mGGA) exchange-correlation functionals by converting them into Laplacian-dependent functionals recently was developed by us and shown to be successful in molecules. It uses an approximate kinetic energy density functional (KEDF) parametrized to Kohn-Sham results (not experimental data) on a small training set. Here we present extensive validation calculations on periodic solids that demonstrate that the same deorbitalization with the same parametrization also is successful for those extended systems. Because of the number of stringent constraints used in its construction and its recent prominence, our focus is on the SCAN meta-GGA. Coded in VASP, the deorbitalized version, SCAN-L, can be as much as a factor of three faster than original SCAN, a potentially significant gain for large-scale ab initio molecular dynamics.

I. BACKGROUND AND MOTIVATION

Accuracy, generality, and computational cost are competing priorities in the unrelenting search for theoretical constructs on which to base predictive condensed matter calculations. A critical problem is to predict the stable zero-temperature lattice structure of a crystal, its cohesive energy, its bulk modulus, and fundamental gap. Treatment of other physical properties (e.g., phonon spectra, transport coefficients, response functions, etc.) is, in principle at least, built upon ingredients drawn from solution of that central problem.

Beginning about four decades ago, the dominant paradigm which emerged for treating that central problem is density functional theory (DFT)[1–3] in its Kohn-Sham (KS)[4,5] form. For an N_e electron system, the KS procedure recasts the DFT variational problem as one for a counterpart non-interacting system which has its minimum at the physical system ground state energy E_0 and electron number density $n_0(\mathbf{r})$. The computational problem is to solve the KS equation

$$\{-\tfrac{1}{2}\nabla^2 + v_{\mathrm{KS}}([n];\mathbf{r})\}\varphi_i(\mathbf{r}) = \epsilon_i\varphi_i(\mathbf{r}) . \tag{1}$$

(in Hartree atomic units). The KS potential is

$$v_{\mathrm{KS}} = \delta(E_{\mathrm{Ne}} + E_{\mathrm{H}} + E_{\mathrm{xc}})/\delta n \equiv v_{\mathrm{ext}} + v_{\mathrm{H}} + v_{\mathrm{xc}} \tag{2}$$

where we have assumed, as appropriate for clamped nucleus solids, that the external potential, $v_{\mathrm{ext}} = \delta E_{\mathrm{Ne}}/\delta n$, is from nuclear-electron attraction. The electron-electron Coulomb interaction energy customarily is partitioned as shown, namely the classical Coulomb repulsion (Hartree energy), E_{H}, and the residual exchange-correlation (XC) piece E_{xc}. Note that E_{xc} also contains the kinetic energy correlation contribution, namely the difference between the interacting and non-interacting system kinetic energies (T and T_s respectively).

The only term of this problem which is not known explicitly is E_{xc}. Great effort has gone into constructing approximations to it. A convenient classification, the Perdew-Schmidt Jacob's ladder[6], proceeds by the number and type of ingredients, e.g. spatial derivatives, non-interacting kinetic energy density, exact exchange, etc. For present purposes the relevant rungs of that ladder are the generalized gradient approximation (GGA; dependent upon $n(\mathbf{r})$ and $\nabla n(\mathbf{r})$) and conventional meta-GGA functionals, which also depend upon the non-interacting KE density,

$$t_{\mathrm{s}}^{\mathrm{orb}}(\mathbf{r}) := \tfrac{1}{2}\sum_{i=1}^{N_e}|\nabla\varphi_i(\mathbf{r})|^2 . \tag{3}$$

(For simplicity of exposition, we have assumed unit occupancy and no degeneracy of KS orbitals.) There also are meta-GGA functionals that depend on $\nabla^2 n$ rather than $t_{\mathrm{s}}^{\mathrm{orb}}$ (see for example Refs. 7–10). For reasons that will become evident shortly, we distinguish that class as "mGGA-L".

Most often (but not universally) mGGA XC functionals use $t_{\mathrm{s}}^{\mathrm{orb}}$ in the combination

$$\alpha[n] := (t_{\mathrm{s}}^{\mathrm{orb}}[n] - t_W[n])/t_{TF}[n] := t_\theta/t_{TF} \tag{4}$$

as a way to detect chemically distinct spatial regions[11]. The other ingredients in $\alpha[n]$ are the Thomas-Fermi[12,13] and von Weizsäcker[14] KE densities:

$$t_{TF} = c_{TF}n^{5/3}(\mathbf{r}) \quad , \quad c_{TF} := \frac{3}{10}(3\pi^2)^{2/3} \tag{5}$$

$$t_W = \frac{5}{3}t_{TF}s^2 . \tag{6}$$

The dimensionless reduced density gradient used in GGAs and mGGAs is

$$s := \frac{|\nabla n(\mathbf{r})|}{2(3\pi^2)^{1/3}n^{4/3}(\mathbf{r})} . \tag{7}$$

Because $\alpha[n]$ is explicitly orbital dependent, the mGGA XC potential, $v_{\mathrm{xc}} = \delta E_{\mathrm{xc}}/\delta n$ is not calculable directly but instead must be obtained as an optimized effective potential (OEP)[15–18]. The computational cost of OEP calculations is high enough that the procedure

rarely is used in practice. Instead the so-called generalized Kohn-Sham (gKS) scheme is used. In gKS, the variational procedure is done with respect to the orbitals, not n. That delivers a set of non-local potentials $\delta E_{xc}/\delta \varphi_i$ rather than the local v_{xc}. For a mGGA, the KS and gKS schemes are inequivalent[19,20], a matter of both conceptual and practical consequences.

Very recently we have shown[21] that it is possible, at least for molecules, to convert several successful mGGAs to Laplacian-level XC functionals, mGGA-L, by a constraint-based deorbitalization strategy. The scheme is to evaluate $\alpha[n]$ with an *orbital-independent* approximation for t_θ, i.e., for $t_s^{orb}[n]$. This is done with a KE density functional (KEDF) that is parametrized to KS calculations on a small data set (18 atoms). The parametrization is required to satisfy known constraints on the KE density. When tested against standard molecular datasets for a considerable variety of properties, certain deorbitalized (Laplacian-level) versions of three well-known meta-GGAs, MVS[22], TPSS[23], and SCAN[24], gave as good or better results than the originals. Details are in Ref. 21. The pertinent point here is that at least one successful deorbitalization could be found for each of those three meta-GGAs.

An obvious, crucial challenge is whether the *identical* deorbitalization of a mGGA that is successful on those molecular tests can deliver equally satisfactory results on bulk solid validation tests. (Deorbitalization candidates that were unsuccessful for molecules obviously are irrelevant to this issue of transferability and broad utility.) If that were to be true, then the deorbitalization strategy would be validated as truly successful in that it is for general ground states, not restricted to a particular state of aggregation. Here we focus exclusively on the SCAN[24] functional because of recent intense exploration of its broad efficacy on a considerable variety of molecular and solid systems. In short, we show that indeed SCAN-L, which is SCAN deorbitalized with the PCopt Laplacian KEDF from [21], is essentially as accurate on a variety of solid validation tests as the original SCAN. The deorbitalization strategy applied to SCAN thus is validated as general, not specific to finite, self-bound systems.

For context, since our work on molecular validation[21], we have become aware of two other studies involving deorbitalization. Bienvenu and Knizia[25] used the Perdew-Constantin[26] deorbitalization of the TPSS[23] XC functional as published to serve as a vehicle to bring meta-GGA XC functionals within the scope of robust Coulomb fitting[27] as done in auxiliary density functional theory[28] for molecules. Nothing new was added about deorbitalization *per se*, so that paper is only tangential to the present work. Immediately after concluding the present study we learned of a comparison of the Ref. 21 deorbitalization candidates (and others) on a variety of solids[29]. The emphasis of Ref. 29 is on variability and sensitivity in solid system outcomes with respect to deorbitalization procedure choice. Broadly speaking that study therefore

is the counterpart in solids to the molecular exploration of Ref. 21. Though intrinsically interesting, it is not the focus here. Their conclusions, however, are consistent with ours regarding SCAN-L transferability to solids. A bit more detail is provided in Conclusions, Sect. VI.

In order, the sections which follow give computational details (Sect. II), numerical results (Sect. III), interpretive comparison of original and deorbitalized quantities such as $\alpha[n]$ (Sect. IV), computational performance (Sect. V), and brief conclusions (Sect. VI). Some Supplemental Information also is provided, as noted.

II. COMPUTATIONAL DETAILS

The deorbitalized SCAN (SCAN-L) used in all calculations discussed here is precisely the form and parametrization given in Ref. 21 as the faithful case, i.e. with the PCopt KEDF representation of the bonding-region discrimination functional $\alpha[n(\mathbf{r})]$.

All computations presented in this work were performed with a locally modified version of the Vienna *ab initio* Simulation Package (VASP)[30–32]. Two separate implementations of the deorbitalized scheme were coded. One used the mGGA trunk of VASP, modified as necessary to handle the Laplacian-dependence. Despite being in the conventional mGGA trunk, the deorbitalized modification used the KS procedure, not gKS. The second version used the GGA trunk, augmented to include the Laplacian in the one place it appears, $\alpha[n]$, and its derivative appearance in v_{KS}. These coding differences have pronounced computational performance consequences, as discussed in Sect. V.

The PAW data sets[33] utilized correspond to the PBE 5.4 package and are summarized in Table I. We note that the use of inconsistent PAW data sets (PBE with SCAN) follows precedent. This is because, to our knowledge, there is no alternative; no SCAN-based PAW data set is available for VASP. These PAW data sets contain information about the core kinetic energy density needed by SCAN[24]. There are two exceptions, H and Li, for which the selected PAW data sets are all-electron but violate the requirement given in the VASP Wiki[34]. We found, nevertheless, that the equilibrium lattice constants for LiH, LiF, and LiCl from an equation of state fitted (see below) to calculations that used those PAW data sets are quite sensible. It is important to mention that in order to obtain the same equilibrium lattice constants from the stress tensor values as from the equation of state fitting the *patch #1*[35] needs to be applied to VASP.

Though the use of ultra-soft pseudopotentials has been somewhat de-emphasized in recent years in favor of PAWs, for the sake of completeness we have done ultra-soft pseudopotential counterpart solid validation studies to those reported below for PAWs. The VASP ultra-soft pseudopotential library was used. Those results are tabulated in the Supplemental Information[36] and discussed briefly in Sect. VI.

The default energy cutoff (VASP variable `ENCUT`) was overridden and set to 800 eV, except for calculations involving Li. In those, the cutoff was increased to 1000 eV for LiCl and LiF, and to 1200 eV for Li.

The precision parameter in VASP was set to "accurate" (`PREC=A`) and the minimization algorithm used an "all-band simultaneous update of orbitals" conjugate gradient method (`ALGO=A`). Non-spherical contributions within the PAW spheres were included self-consistently (`LASPH=.TRUE.`).

For hexagonal close-packed structures we used the ideal c/a ratio. For graphite and hexagonal boron nitride, we fixed the intralayer lattice constant to its experimental value and varied only the interlayer lattice constant.

Brillouin zone integrations were performed on ($17 \times 17 \times 17$) Γ-centered symmetry reduced Monkhorst-Pack[37] k-meshes using the tetrahedron method with Blöchl corrections[38].

The equilibrium lattice constants a_0 and bulk moduli B_0 at $T = 0K$ were determined by calculating the total energy per unit cell in the range $V_0 \pm 10\%$ (where V_0 is the equilibrium unit cell volume), followed by a twelve-point-fit to the stabilized jellium equation of state (SJEOS)[39]. The SJEOS is

$$E(V) = \alpha \left(\frac{V_0}{V}\right) + \beta \left(\frac{V_0}{V}\right)^{2/3} + \gamma \left(\frac{V_0}{V}\right)^{1/3} + \omega . \quad (8)$$

A linear fit to Eq. (8) yields parameters $\alpha_s = \alpha V_0$, $\beta_s = \beta V_0^{2/3}$, $\gamma_s = \gamma V_0^{1/3}$ and ω, from which

$$V_0 = \left(\frac{-\beta_s + \sqrt{\beta_s^2 - 3\alpha_s \gamma_s}}{\gamma_s}\right)^3 , \quad (9)$$

$$B_0 = \frac{18\alpha + 10\beta + 4\gamma}{9V_0} . \quad (10)$$

To obtain cohesive energies, approximate isolated atom energies were calculated from a $14 \times 15 \times 16$ Å^3 cell. The lowest energy configuration was sought by allowing spin-polarization and breaking spherical symmetry, but without spin-orbit coupling.

III. NUMERICAL RESULTS

Table III compares static-crystal lattice constants and cohesive energies of 55 solids and Table IV compares bulk moduli of 44 solids computed with the orbital-dependent SCAN and its deorbitalized version SCAN-L. Experimental values shown in Table III were taken from Ref. 40. Those in Table IV were taken from Ref. 41. The overall excellent agreement between the values obtained with SCAN and SCAN-L for all three properties indicate that SCAN-L provides a *faithful* reproduction of the SCAN potential energy surfaces near equilibrium for these systems.

Figure 1 depicts the correlation between SCAN and SCAN-L results for each of the three properties and lists the regression coefficients. (The Supplemental Material[36] provides an alternative display as a system-by-system scatter plot of percentage errors for SCAN versus SCAN-L.) Outliers differing more than $\pm 10\%$ are indicated by their chemical symbol. It is readily apparent from Figure 1 that SCAN-L predicts Pt, Rh, and Ir to be more compressible than does the original SCAN functional. On the other hand, SCAN-L predicts Al, LiCl, K, and Rb to be less compressible (these solids are not highlighted in Figure 1 due to cluttering). At the resolution of that figure, there are no serious outliers for equilibrium lattice constant. In fact, the differences between lattice constants predicted by SCAN and SCAN-L are 1% or less for each one of the solids. There are a few outliers in the cohesive energies set. However, it is notable that there is no systematic under- or overbinding from SCAN-L with respect to SCAN values of E_{coh}. The ground-state configurations of all elements were the same with SCAN and SCAN-L, however, we must note that one must start from a previously converged PBE density to obtain the lowest lying state of Hf with SCAN-L. Because the E_{coh} outliers are d and f elements, the most plausible reason for the differences is the difference in density resulting from KS versus gKS band-structures and associated occupancies near the fermi level.

Table V displays KS band gaps for SCAN-L compared to those from SCAN. As expected, the SCAN-L band gap values always are less than or equal to those from the orbital-dependent SCAN. This systematic difference arises because the SCAN-L exchange-correlation potential is a local multiplicative one, whereas the one from orbital-dependent SCAN is non-multiplicative[19]. In other words, the difference in KS band gaps is consistent with the difference between KS and generalized gKS methods. If SCAN-L is a *faithful* deorbitalization of SCAN, then the SCAN-L exchange-correlation potential should be a good approximation to the SCAN OEP (which, so far as we know, has not been generated for any solid), Thus, the SCAN-L KS band gaps should agree reasonably well with the values obtained in Ref. 19 for the Krieger-Li-Iafrate (KLI)[42] approximation to the OEP of SCAN. To facilitate such comparison, Table V shows both the "SCAN(BAND)" and "SCAN(KLI)" band gaps reported in Ref. 19. "SCAN(BAND)" results are all-electron gKS values from the BAND code[43]. The SCAN band gaps computed here with VASP and PAWs are smaller than those obtained with the BAND code as reported in Ref. 19. Presumably that is a consequence of the PAWs and the difference in basis sets. However, there is no systematic deviation of the SCAN-L KS band gaps from the SCAN(KLI) ones. Most are close, with the two outliers, in a relative sense, being GaAs and InP: 0.33 eV and 0.59 eV from SCAN-L versus 0.45 eV and 0.77 eV from SCAN(KLI), respectively. It therefore seems that the SCAN-L potential is at least a reasonably good approximation to the SCAN OEP.
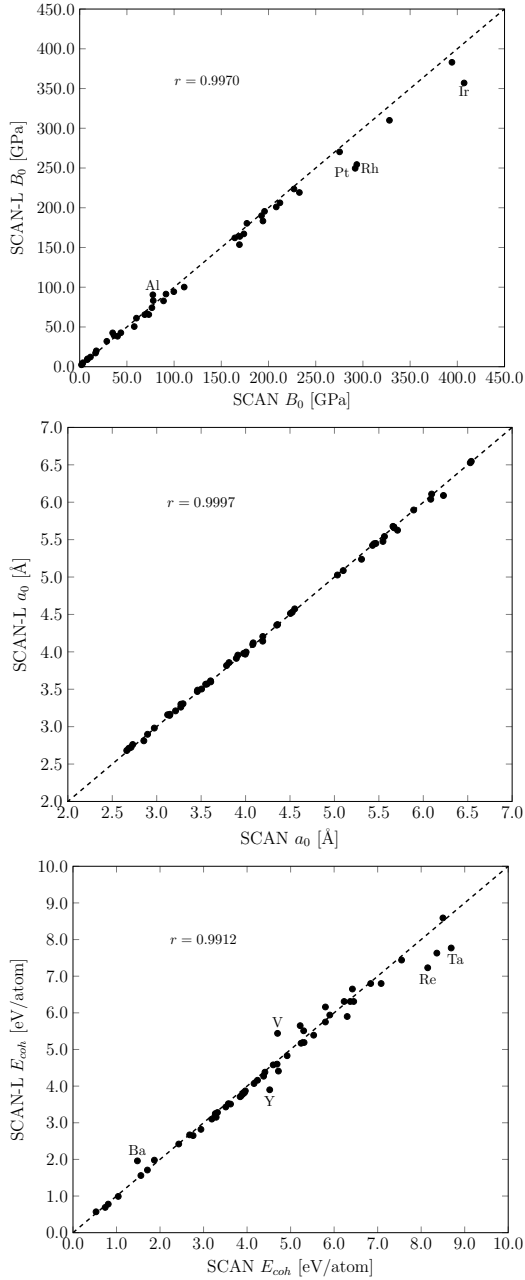
FIG. 1. Comparison between SCAN and SCAN-L bulk moduli B_0 (top), static-crystal lattice constants a_0 (middle), and cohesive energies E_{coh} (bottom). A dashed line with slope 1 and Pearson correlation coefficient r is shown in each of the three plots.

One of the features of SCAN that has been emphasized in the literature is its ability to capture intermediate-distance correlation effects in weakly bonded systems such as graphite and hexagonal boron nitride (h-BN)[40,44]. Table VI shows the interlayer binding energy E_b and interlayer lattice constant c for these two systems from SCAN and SCAN-L as well as reference values from Ref. 40. E_b is small, thus particularly sensitive to formal and computational differences. Nevertheless SCAN-L re-
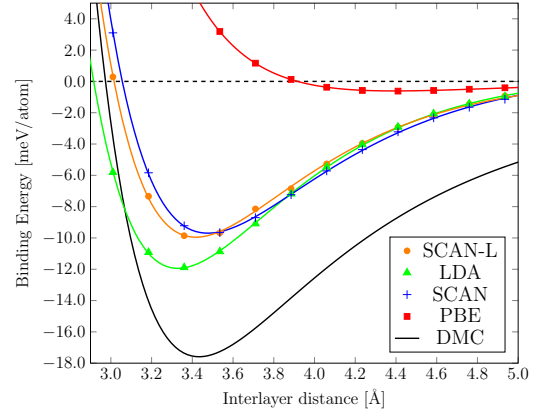

FIG. 2. Graphene bilayer interplanar binding (meV/atom) as computed with LDA, PBE, SCAN, and SCAN-L XC functionals. A fit to diffusion quantum Monte Carlo (DMC) data[48] is shown as reference.

produces the SCAN E_b result for graphite and h-BN to less than 5.0% discrepancy. The SCAN-L c values are somewhat closer to the reference ones but still agree to less than 2.5% difference with the SCAN ones. Note, however, that our SCAN binding energies for Graphite and h-BN are 10% smaller than those reported in Reference [40].

It is also significant for use of van der Waals corrections[40,46] that SCAN-L reproduces the SCAN binding curve $E_b(c)$ for a graphene bilayer quite well. In Fig. 2 we show the binding curves for LDA, PBE[47], SCAN and SCAN-L XC functionals compared to a diffusion quantum Monte Carlo (DMC) reference[48]. The SCAN-L functional is able to recover as much of the binding "lost" by PBE and other GGA-type functionals (relative to DMC or even LDA) as does SCAN. The interlayer separation predicted by SCAN (3.48 Å) and SCAN-L (3.41 Å) are in good agreement to the DMC-fit prediction (3.42 Å).

IV. INTERPRETIVE RESULTS

How the *faithful* deorbitalization is achieved in SCAN-L can be understood by how well α is approximated by the kinetic energy density functional utilized. Figure 3 shows the comparison between the orbital-dependent α Eq. (4) and the approximation that results from use of the PCopt KEDF in deorbitalizing α in SCAN[21]. Details of the PCopt parametrization are in that reference. The three systems selected as examples in Fig. 3 were chosen because they span the bonding situations among which α is supposed to discriminate. The BeH radical has $\alpha \approx 0$ as is true of most covalently bounded systems. The sodium dimer has $\alpha \approx 1$ as in most metallic systems. The stacked benzene dimer is representative of weakly bound systems for which $\alpha \gg 1$ is typical. Generally the deorbitalized αs follow their orbital-dependent

TABLE I. PAWs used in the present work. The energy cut-offs E_{cut} (eV) shown are the default for each PAW and were overridden as discussed in the text.

Element	Name	Valence	E_{cut}
H	H_h_GW	$1s$	700
Li	Li_AE_GW	$1s2s$	433
B	B	$2s2p$	319
C	C_GW_new	$2s2p$	414
N	N_GW_new	$2s2p$	421
O	O_GW_new	$2s2p$	434
F	F_GW_new	$2s2p$	487
Na	Na_pv	$2p3s$	373
Mg	Mg_sv_GW	$2s2p3s$	430
Al	Al_GW	$3s3p$	240
Si	Si_GW	$3s3p$	547
P	P_GW	$3s3p$	255
S	S_GW	$3s3p$	259
Cl	Cl_GW	$3s3p$	262
K	K_pv	$3p4s$	249
Ca	Ca_pv	$3p4s$	119
Sc	Sc_sv_GW	$3s3p3d4s$	379
Ti	Ti_sv_GW	$3s3p3d4s$	384
V	V_sv_GW	$3s3p3d4s$	382
Fe	Fe_sv_GW	$3s3p3d4s$	388
Co	Co_sv_GW	$3s3p3d4s$	387
Ni	Ni_sv_GW	$3s3p3d4s$	390
Cu	Cu_GW	$3d4s$	417
Ga	Ga_d_GW	$3d4s4p$	404
Ge	Ge_d_GW	$3d4s4p$	375
As	As_GW	$4s4p$	208
Rb	Rb_sv	$4s4p5s$	424
Sr	Sr_sv	$4s4p5s$	229
Y	Y_sv_GW	$4s4p4d5s$	340
Zr	Zr_sv_GW	$4s4p4d5s$	346
Nb	Nb_sv_GW	$4s4p4d5s$	354
Mo	Mo_sv_GW	$4s4p4d5s$	345
Tc	Tc_sv_GW	$4s4p4d5s$	351
Ru	Ru_sv_GW	$4s4p4d5s$	348
Rh	Rh_sv_GW	$4s4p4d5s$	351
Pd	Pd_pv	$4p4d5s$	250
Ag	Ag_GW	$4d5s$	250
In	In_d_GW	$4d5s5p$	279
Sn	Sn_d_GW	$4d5s5p$	260
Sb	Sb_GW	$5s5p$	172
Cs	Cs_sv_GW	$5s5p6s$	198
Ba	Ba_sv_GW	$5s5p6s$	237
Hf	Hf_sv_GW	$5p6s6d$	283
Ta	Ta_sv_GW	$5p6s6d$	286
W	W_sv_GW	$5p5d6s$	317
Re	Re_sv_GW	$5p5d6s$	317
Os	Os_sv_GW	$5p5d6s$	320
Ir	Ir_sv_GW	$5p5d6s$	320
Pt	Pt_pv	$5p5d6s$	295
Au	Au_GW	$5d6s$	248

TABLE II. Strukturbericht symbols of the 57 solids used in the present work: A1 face-centered cubic, A2 body-centered cubic, A3 hexagonal close-packed, A9 hexagonal unbuckled graphite, B1 rock salt, B3 zinc blende, and B_k hexagonal boron nitride.

Solid	Symbol	Solid	Symbol	Solid	Symbol
C	A4	NaF	B1	Hf	A3
Si	A4	NaCl	B1	V	A2
Ge	A4	MgO	B1	Nb	A2
Sn	A4	Li	A2	Ta	A2
SiC	B3	Na	A2	Mo	A2
BN	B3	K	A2	W	A2
BP	B3	Rb	A2	Tc	A3
AlN	B3	Cs	A2	Re	A3
AlP	B3	Ca	A1	Ru	A3
AlAs	B3	Ba	A2	Os	A3
GaN	B3	Sr	A1	Rh	A1
GaP	B3	Al	A1	Ir	A1
GaAs	B3	Fe	A2	Pd	A1
InP	B3	Co	A1	Pt	A1
InAs	B3	Ni	A1	Cu	A1
InSb	B3	Sc	A3	Ag	A1
LiH	B1	Y	A3	Au	A1
LiF	B1	Ti	A3	C	A9
LiCl	B1	Zr	A3	BN	B_k

differences between the exact and approximate αs might be observed in the tails of the density. Those are almost nonexistent in condensed systems near equilibrium and they prove to be inconsequential for molecules (which is why such points are screened out in most molecular computational packages). In short, where it counts in both solids and molecules, the PCopt function reproduces the behavior of the original SCAN α.

V. COMPUTATIONAL PERFORMANCE

To obtain a quantitative picture of the performance of GGA and mGGA calculations in VASP, we prepared a fully sequential (serial) version compiled in profiling mode and linked to the Intel Math Kernel and Fast Fourier Transform libraries. Two variants were compiled, original and with SCAN-L included. Within the original variant, three calculations were done: PBE using the GGA trunk (`GGA=PBE`), PBE using the mGGA trunk (`METAGGA=PBE`) and SCAN (`METAGGA=SCAN`). Correspondingly in the SCAN-L coded variant, the four were PBE using the extended GGA trunk (`GGA=PE`), PBE using the modified mGGA trunk (`METAGGA=PBE`), SCAN-L using the extended GGA trunk (`GGA=SL`) and SCAN-L using the modified mGGA trunk (`METAGGA=SCANL`).

The test system was diamond carbon at a lattice constant, $a_0 = 3.560$ Å, near the SCAN-L equilibrium value. Calculations used a 600 eV planewave cutoff, the all-bands conjugate gradient minimization (`ALGO=A`), aspherical corrections (`LASPH=.TRUE.`), doubling of the Fourier grid (`ADDGRID=.TRUE.`) and the tetrahedron method with

counterparts closely both within and outside the bonding regions. Perceptible differences can be noted for the benzene dimer at the mid-point of the interplanar axis. However, even though that deorbitalized α is almost 50 % of the exact one, the difference between SCAN and SCAN-L enhancement factors is less than 5 %. Larger

TABLE III. Static-lattice lattice constant, a_0 (Å), and cohesive energy, E_{coh} (eV/atom), comparisons for 55 solids. The experimental values ("Expt."), from Ref. 40, include zero-point effects.

| Solid	a_0			E_{coh}		
	Expt.	SCAN	SCAN-L	Expt.	SCAN	SCAN-L
C	3.553	3.551	3.567	7.55	7.55	7.44
Si	5.421	5.429	5.423	4.68	4.69	4.60
Ge	5.644	5.668	5.667	3.89	3.94	3.82
Sn	6.477	6.540	6.546	3.16	3.27	3.25
SiC	4.346	4.351	4.357	6.48	6.45	6.31
BN	3.592	3.606	3.612	6.76	6.84	6.80
BP	4.525	4.525	4.530	5.14	5.31	5.19
AlN	4.368	4.360	4.364	5.85	5.80	5.75
AlP	5.451	5.466	5.449	4.32	4.24	4.16
AlAs	5.649	5.671	5.659	3.82	3.84	3.71
GaN	4.520	4.505	4.513	4.55	4.41	4.38
GaP	5.439	5.446	5.445	3.61	3.62	3.51
GaAs	5.640	5.659	5.677	3.34	3.29	3.15
InP	5.858	5.892	5.896	3.47	3.19	3.10
InAs	6.047	6.094	6.109	3.08	2.94	2.82
InSb	6.468	6.529	6.528	2.81	2.68	2.67
LiH	3.979	3.997	3.969	2.49	2.43	2.42
LiF	3.972	3.978	3.979	4.46	4.38	4.27
LiCl	5.070	5.099	5.086	3.59	3.51	3.43
NaF	4.582	4.553	4.574	3.97	3.90	3.78
NaCl	5.569	5.563	5.542	3.34	3.26	3.18
MgO	4.189	4.194	4.205	5.20	5.24	5.17
Li	3.443	3.457	3.470	1.67	1.56	1.56
Na	4.214	4.193	4.143	1.12	1.04	0.99
K	5.212	5.305	5.238	0.94	0.81	0.78
Rb	5.577	5.710	5.626	0.86	0.74	0.69
Cs	6.039	6.227	6.090	0.81	0.53	0.57
Ca	5.556	5.546	5.476	1.87	1.87	1.98
Ba	5.002	5.034	5.027	1.91	1.48	1.96
Sr	6.040	6.084	6.040	1.73	1.71	1.71
Al	4.018	4.006	3.997	3.43	3.57	3.52
Fe	2.853	2.855	2.811	4.30	4.60	4.58
Co	3.524	3.505	3.503	4.42	4.72	4.41
Ni	3.508	3.460	3.488	4.48	5.30	5.51
Sc	3.270	3.271	3.261	3.93	3.96	3.87
Y	3.594	3.608	3.503	4.39	4.52	3.90
Ti	2.915	2.897	2.898	4.88	4.92	4.83
Zr	3.198	3.212	3.211	6.27	5.90	5.94
Hf	3.151	3.123	3.159	6.46	6.30	5.90
V	3.021	2.973	2.981	5.35	4.70	5.44
Nb	3.294	3.296	3.306	7.60	6.37	6.31
Ta	3.299	3.272	3.300	8.13	8.69	7.77
Mo	3.141	3.145	3.151	6.86	5.80	6.16
W	3.160	3.149	3.165	8.94	8.36	7.63
Tc	2.716	2.711	2.724	6.88	6.42	6.65
Re	2.744	2.730	2.761	8.05	8.15	7.23
Ru	2.669	2.663	2.681	6.77	6.23	6.31
Os	2.699	2.686	2.710	8.20	8.50	8.59
Rh	3.794	3.786	3.817	5.78	5.22	5.65
Ir	3.831	3.814	3.856	6.99	7.08	6.80
Pd	3.876	3.896	3.913	3.93	4.16	4.07
Pt	3.913	3.913	3.956	5.87	5.53	5.39
Cu	3.595	3.566	3.570	3.51	3.86	3.73
Ag	4.062	4.081	3.913	2.96	2.76	2.65
Au	4.062	4.086	4.120	3.83	3.32	3.28
ME		0.011	0.009		-0.10	-0.17
MAE		0.025	0.024		0.24	0.26
MARE (%)		0.54	0.55		5.91	6.42
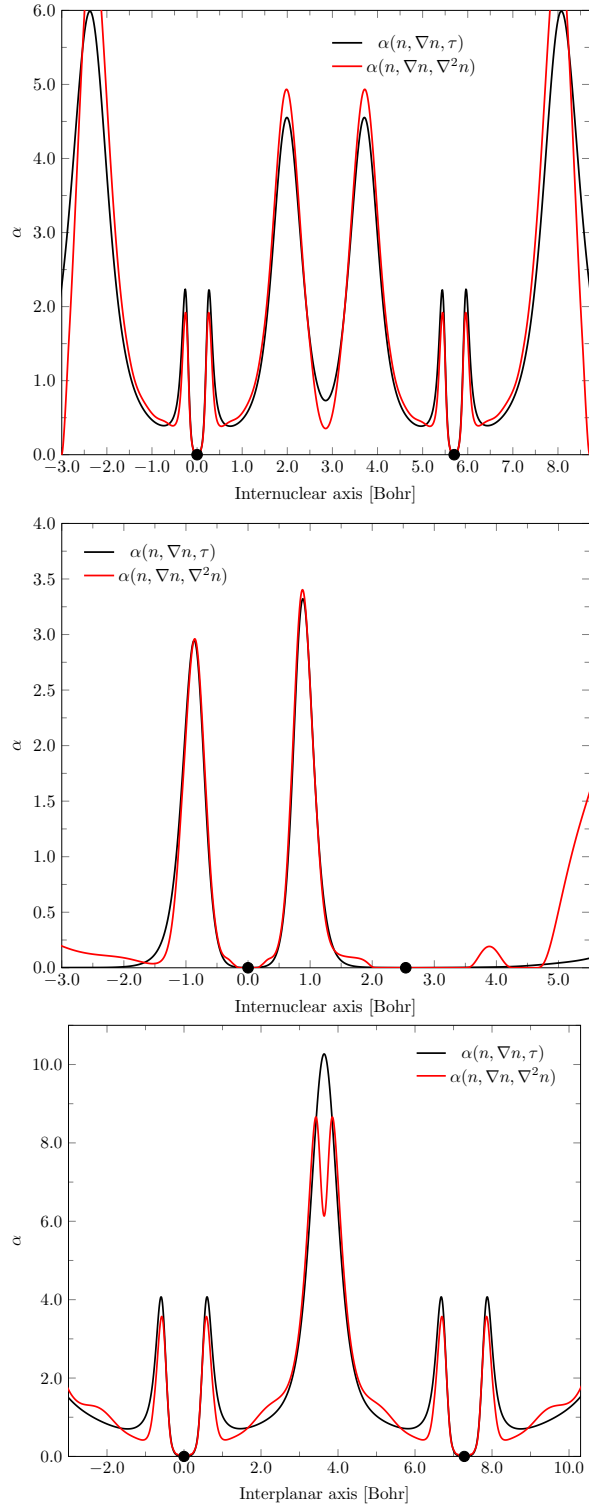
FIG. 3. Orbital-dependent α and its deorbitalized approximation for three representative bonding situations. Na$_2$ (top) exemplifies systems with $\alpha \approx 1$; BeH (middle) exemplifies systems with $\alpha \approx 0$, and the benzene dimer exemplifies those with $\alpha \gg 1$.

TABLE IV. Bulk modulus, B_0 (GPa) of the 44 cubic solids. The experimental values, from Ref. 41, were obtained by subtracting the zero-point phonon effect from the experimental zero-temperature values.

Solid	Expt.	SCAN	SCAN-L
C	454.7	459.9	442.6
Si	101.3	99.7	94.4
Ge	79.4	71.2	66.7
Sn	42.8	40.1	38.3
SiC	229.1	227.0	223.6
BN	410.2	394.3	383.0
BP	168.0	173.9	167.1
AlN	206.0	212.1	206.2
AlP	87.4	91.4	91.4
AlAs	75.0	76.5	74.2
GaN	213.7	194.1	183.3
GaP	89.6	88.8	82.8
GaAs	76.7	73.2	65.6
InP	72.0	68.9	65.5
InAs	58.6	57.8	50.5
InSb	46.1	43.6	42.7
LiH	40.1	36.4	39.4
LiF	76.3	77.9	83.2
LiCl	38.7	34.9	42.6
NaF	53.1	60.1	61.1
NaCl	27.6	28.7	32.0
MgO	169.8	169.6	163.9
Li	13.1	16.8	17.2
Na	7.9	8.0	8.9
K	3.8	3.4	5.0
Rb	3.6	2.7	3.3
Cs	2.3	1.9	2.4
Ca	15.9	17.6	20.0
Ba	10.6	8.3	9.9
Sr	12.0	11.4	12.2
Al	77.1	77.5	90.5
Ni	192.5	232.7	219.2
V	165.8	195.8	195.5
Nb	173.2	177.1	180.4
Ta	202.7	208.2	201.0
Mo	276.2	275.3	270.3
W	327.5	328.1	310.0
Rh	277.1	293.5	254.4
Ir	362.2	407.2	357.0
Pd	187.2	192.6	190.0
Pt	285.5	291.8	249.6
Cu	144.3	164.3	162.1
Ag	105.7	110.7	100.2
Au	182.0	169.2	153.6
ME		3.0	-3.0
MAE		6.9	9.2
MARE (%)		7.2	9.4

Blöchl corrections (`ISMEAR=-5`). These are the same settings as were used for the validation studies, except for the energy cutoff. All calculations converged in 12 scf iterations. It is important to note that our VASP implementation does compute the term $\nabla^2 \left(\partial \epsilon_{xc}/\partial \nabla^2 n \right)$. This is distinct from our SCAN-L implementation in NWChem[49] reported in Ref. 21, where integration by

TABLE V. Band gap (eV) of 21 insulators and semiconductors. Experimental lattice parameters were used with all functionals. Experimental band gaps and lattice constants were taken from Ref. 45. The SCAN(BAND) and SCAN(KLI) results are from Ref. 19.

Solid	Expt.	SCAN	SCAN-L	SCAN(BAND)	SCAN(KLI)
C	5.50	4.54	4.22	4.58	4.26
Si	1.17	0.82	0.80	0.97	0.78
Ge	0.74	0.14	0.00		
SiC	2.42	1.72	1.55		
BN	6.36	4.98	4.66	5.04	4.73
BP	2.10	1.54	1.41	1.74	1.52
AlN	4.90	3.97	3.50		
AlP	2.50	1.92	1.81		
AlAs	2.23	1.74	1.59		
GaN	3.28	1.96	1.49		
GaP	2.35	1.83	1.72	1.94	1.72
GaAs	1.52	0.77	0.33	0.80	0.45
InP	1.42	1.02	0.59	1.06	0.77
InAs	0.42	0.00	0.00		
InSb	0.24	0.00	0.00		
LiH	4.94	3.66	3.69		
LiF	14.20	10.10	9.16	9.97	9.11
LiCl	9.40	7.33	6.80		
NaF	11.50	7.14	6.45		
NaCl	8.50	5.99	5.59	5.86	5.25
MgO	7.83	5.79	4.92	5.62	4.80
ME		-1.26	-1.58		
MAE		1.26	1.58		

TABLE VI. Inter-layer binding energy E_b in meV/Å^2 and inter-layer lattice constant c in Å. The reference E_b values are from RPA calculations and from experiments for c.

Solid	Reference		SCAN		SCAN-L	
	E_b	c	E_b	c	E_b	c
Graphite	18.32	6.70	7.23	6.97	7.37	6.81
h-BN	14.49	6.54	7.66	6.85	7.70	6.72

TABLE VII. Comparative timings for PBE, SCAN, and SCAN-L calculations in the original and modified mGGA and GGA trunks of VASP. All times in seconds. See text for trunk labels.

XC	Trunk	Original Code	Modified Code
PBE	GGA=PE	12.38	12.85
PBE	METAGGA=PBE	36.75	37.57
SCAN	METAGGA=SCAN	61.28	–
SCAN-L	GGA=SL	–	19.32
SCAN-L	METAGGA=SCANL	–	50.72

parts is used to avoid fourth-order derivatives of the density.

Table VII gives the results. Clearly the SCAN-L computational speed in the extended GGA trunk implementation is substantially superior to that for original SCAN. When using the mGGA trunk, SCAN-L performance degrades but the computation is still 20% faster than the original SCAN one.

Analysis of the detailed profiling shows that when a metaGGA functional is requested, VASP first computes results for PBE XC, but then overwrites those results with the corresponding ones from the requested mGGA XC functional. It is not clear why that is done. For mGGAs, additional time is used in computing $\nabla^2 n$, especially on the radial grid within the PAW spheres, even if that Laplacian data actually is un-needed in the requested mGGA XC functional. (Of course, it is used in SCAN-L.) That is done in anticipation of computing the modified Becke-Johnson potential (also called Tran-Blaha 09)[50,51] if requested. Furthermore, the mGGA trunk always assumes spin-polarized densities, resulting in additional time used for spin-unpolarized systems. These three sources of wasted time make the difference between the `GGA=PE` and `METAGGA=PBE` timings.

In the original VASP version, the time difference between `METAGGA=PBE` and `METAGGA=SCAN` arises from the non-locality of the Hamiltonian of a conventional mGGA (as in SCAN). This difference also is present in the comparison of `METAGGA=SCAN` and `METAGGA=SCANL`, but it is mitigated because additional work (compared to PBE) is required to compute $\nabla^2 \left(\partial \epsilon_{xc}/\partial \nabla^2 n \right)$ which is needed for the `METAGGA=SCANL` potential. Implementing SCAN-L as an extension of the GGA trunk saves time because the associated v_{KS} is local. That implementation also avoids wasting time in calculating un-needed PBE results and avoids treating spin-unpolarized systems as spin-polarized ones.

TABLE VIII. Comparison of MAE values from self-consistent vasp calculations with PAWs versus post-SCF wien2k all-electron calculations. a_0 in (Å), E_{coh} in eV/atom, B_0 in GPa.

Code	SCAN			SCAN-L		
	a_0	E_{coh}	B_0	a_0	E_{coh}	B_0
vasp	0.025	0.24	6.9	0.024	0.26	9.2
wien2k	0.030	0.19	7.4	0.028	0.17	7.7

VI. CONCLUSION

The Supplemental Information[36] gives counterparts to Tables III and IV above for vasp calculations that used ultra-soft pseudopotentials instead of PAWs but otherwise were identical to the studies described above. From those counterpart tables, one can see that SCAN-L performs as well with ultra-soft pseudopotentials as with PAWs. Thus the success of the SCAN-L deorbitalization is not dependent upon the specifics of regularization of the nuclear-electron potential for use of a plane-wave basis.

Another probe of possible procedural effects is provided by comparison with the results of Ref. 29. That paper used the WIEN2K[52] full-potential, all-electron code but in post-SCF fashion. That is, the mGGA and mGGA-L expressions for $E_{total}[n]$ were evaluated with KS orbitals from self-consistent solution of Eq. (1) with the PBE GGA exchange-correlation functional[47]. Table I of that paper provides MAE values for SCAN-L (denoted there as "SCAN(PCopt)"). Table VIII compares those values with our self-consistent PAW-based results. Though the MAE values for a_0 and E_{coh} differ between the two codes, the relative shifts between original and de-orbitalized SCAN versions confirm the validity of the PCopt deorbitalization. Indeed, the wien2k post-SCF

comparison of SCAN versus SCAN-L E_{coh} and B_0 MAEs actually is slightly better than for the vasp case. Clearly the choice of basis and associated algorithms does not affect the validity of the PCopt deorbitalization of SCAN.

Overall therefore, we have shown that the SCAN-L functional, a simple orbital-independent form of the sophisticated and much-advertised SCAN functional, can capture essentially all the pertinent details of of SCAN for both in molecules and solids, at least on conventional validation test sets. We believe SCAN-L to be the first example of an orbital-independent functional that provides uniformly rather good performance in these two seemingly irreconcilable domains of aggregation. As such, SCAN-L opens the way for meta-GGA XC accuracy and reliability in orbital-free DFT simulations, a possibility that has not existed heretofore. It also opens the way for much faster ab initio molecular dynamics simulations than are possible with SCAN.

Differences between SCAN-L and SCAN KS band gaps are consistent with well-understood consequence of the difference between KS and gKS solutions. The KS band gaps also provide some evidence that SCAN-L provides a reasonable approximation to the OEP for SCAN. Direct comparison with the exact OEP (rather than the KLI approximation) would be welcome. The performance of SCAN-L in combination with van der Waals correction schemes also remains to be investigated.

* dmejiarodriguez@ufl.edu
† trickey@qtp.ufl.edu

[1] P. Hohenberg and W. Kohn, Phys. Rev. **136**, B864 (1964).
[2] M. Levy, Proc. Natl. Acad. Sci. USA **76**, 6062 (1979).
[3] E.H. Lieb, Int. J. Quantum Chem. **24**, 243 (1983).
[4] W. Kohn and L.J. Sham, Phys. Rev. **140**, A1133 (1965).
[5] *Density Functional Theory: An Advanced Course*, E. Engel and R.M. Dreizler (Springer-Verlag Berlin, Berlin, 2011) and refs. therein.
[6] J.P. Perdew and K. Schmidt, A.I.P. Conf. Proc. **577**, 1 (2001).
[7] E. Engel and S.H. Vosko, Phys. Rev. B **50**, 10498 (1994).
[8] M. Filatov and W. Thiel, Phys. Rev. A **57**, 189 (1998).
[9] E.I. Proynov, E. Ruiz, A. Vela and D.R. Salahub, Int. J. Quantum Chem. **56**, 61 (1995).
[10] A.A. Cancio, C.E. Wagner and S.A. Wood, Int. J. Quantum Chem. **112**, 3796 (2012).
[11] J. Sun, B. Xiao, and A. Ruzsinszky, J. Chem. Phys. **137**, 051101 (2012).
[12] L.H. Thomas, Proc. Cambridge Phil. Soc. **23**, 542 (1927).
[13] E. Fermi, Atti Accad. Nazl. Lincei **6**, 602 (1927).
[14] C.F. von Weizsäcker, Z. Phys. **96**, 431 (1935).
[15] M. Städele, J.A. Majewski, P. Vogl and A. Görling, Phys. Rev. Lett. **79**, 2089 (1997)
[16] T. Grabo, T. Kreibich and E.K.U. Gross, Molec. Eng. **7**, 27 (1997).
[17] T. Grabo, T. Kreibach, S. Kurth, and E.K.U. Gross, in *Strong Coulomb Correlations in Electronic Structure: Beyond the Local Density Approximation*, V.I. Anisimov ed. (Gordon and Breach, Tokyo, 2000) 203.
[18] A. Heßelmann and A. Görling, Chem. Phys. Lett. **455**, 110 (2008) and refs. therein.
[19] Z-h. Yang, H. Peng, J. Sun, and J.P. Perdew, Phys. Rev. B **93**, 205205 (2016)
[20] J.P. Perdew, W. Yang, K. Burke, Z. Yang, E.K.U. Gross, M. Scheffler, G.E. Scuseria, T.M. Henderson, I.Y. Zhang, A. Ruzsinszky, H. Peng, J. Sun, E. Trushin, and A. Görling, Proc. Nat. Acad. Sci. (USA) **114**, 2801 (2017).
[21] Daniel Mejía-Rodríguez and S.B. Trickey, Phys. Rev. A **96**, 052512 (2017).

[22] J. Sun, J.P. Perdew, and A. Ruzsinszky, Proc. Nat. Acad. Sci. (USA) **112**, 685 (2015).

[23] J. Tao, J.P. Perdew, V.N. Staroverov, and G.E. Scuseria, Phys. Rev. Lett. **91**, 146401 (2003).

[24] J. Sun, A. Ruzsinszky and J.P. Perdew, Phys. Rev. Lett. **115**, 036402 (2015).

[25] A.V. Bienvenu and G. Knizia, J. Chem. Th. Comput. **14**, 1297 (2018).

[26] J.P. Perdew and L.A. Constantin, Phys. Rev. B **75**, 155109 (2007).

[27] B.I. Dunlap, N. Rösch, and S.B. Trickey, Mol. Phys. **108**, 3167 (2010) and refs. therein.

[28] B. Zuñiga-Gutierrez and A.M. Köster, Mol. Phys. **114**, 1026 (2016).

[29] F. Tran, P. Kovács, L. Kalantari, G.K.H. Madsden, and P. Blaha, arXiv 1807.07302v1

[30] G. Kresse and J. Hafner, Phys. Rev. B **47**, 558 (1993); ibid. **49**, 14251 (1994).

[31] G. Kresse and J. Furthmüller, Comput. Mat. Sci. **6**, 15 (1996).

[32] G. Kresse and J. Furthmüller, Phys. Rev. B **54**, 11169 (1996).

[33] G. Kresse and D. Joubert, Phys. Rev. B **59**, 1758 (1999).

[34] http://cms.mpi.univie.ac.at/wiki/index.php/METAGGA

[35] https://www.vasp.at/index.php/news/bugfixes/119-bugfix-patch-1-for-vasp-5-4-4-18apr17

[36] Supplemental Material link here.

[37] H.J. Monkhorst and J. Pack, Phys. Rev. B **13**, 5188 (1976).

[38] P.E. Blöchl, O. Jepsen and O.K. Andersen, Phys. Rev. B **49**, 16223 (1994).

[39] A.B. Alchagirov, J.P. Perdew, J.C. Boettger, R.C. Albers and C. Fiolhais, Phys. Rev. B. **63** 224115 (2001).

[40] H. Peng, Z.-H. Yang, J.P. Perdew and J. Sun, Phys. Rev. X **6**, 041005 (2016).

[41] F. Tran, J. Stelzl and P. Blaha, J. Chem. Phys. **144**, 204120 (2016).

[42] J.B. Krieger, Y. Li, and G.J. Iafrate Int. J. Quantum Chem. **41**, 481 (1992)

[43] G. te Velde and E.J. Baerends, Phys. Rev. B **44**, 7888 (1991); G. Wiesenekker and E.J. Baerends, J. Phys.: Condens. Matter **3**, 6721 (1991); P. H.T. Philipsen, G. te Velde, E.J. Baerends, J.A. Berger, P.L. de Boeij, M. Franchini, J.A. Groeneveld, E.S. Kadantsev, R. Klooster, F. Kootstra, P. Romaniello, D.G. Skachkov, J.G. Snijders, C.J.O. Verzijl, J.A. Celis Gil, J.M. Thijssen, G. Wiesenekker, and T. Ziegler, BAND2017, SCM, Theoretical Chemistry, Vrije Universiteit, Amsterdam, The Netherlands, 2017.

[44] J. Sun, R.C. Remsing, Y. Zhang, Z. Sun, A. Ruzsinszky, H. Peng, Z. Yang, A. Paul, U. Waghmare, X. Wu, M.L. Klein, and J.P. Perdew, Nature Chemistry **8**, 831 (2016).

[45] F. Tran and P. Blaha, J. Phys. Chem. A **121**, 3318 (2017).

[46] J. Hermann and A. Tkatchenko, J. Chem. Theory Comput. **14**, 1361 (2018).

[47] J.P. Perdew, K. Burke and M. Ernzerhof, Phys. Rev. Lett. **77**, 3865 (1996).

[48] E. Mostaani, N.D. Drummond and V.I. Fal'ko, Phys. Rev. Lett. **115**, 115501 (2015).

[49] M. Valiev, E.J. Bylaska, N. Govind, K. Kowalski, T.P. Straatsma, H.J.J. Van Dam, D. Wang, J. Nieplocha, E. Apra, T.L. Windus, and W. de Jong, Comput. Phys. Commun. **181**, 1477 (2010).

[50] A.D. Becke and E.R. Johnson, J. Chem. Phys. **124**, 221101 (2006).

[51] F. Tran and P. Blaha, Phys. Rev. Lett. **102**, 226401 (2009).

[52] P. Blaha, K. Schwarz, G.K.H. Madsen, D. Kvasnicka, J. Luitz, R. Laskowski, F. Tran, and L.D. Marks, *WIEN2K: An Augmented Plane Wave plus Local Orbitals Program for Calculating Crystal Properties* (Vienna University of Technology, Austria, 2018).